The FEBS Journal

FEBS PRESS science publishing by scientists

Salt bridge interactions within the β_2 integrin α_7 helix mediate force-induced binding and shear resistance ability

Xiao Zhang[1,2,3,4,†], Linda Li[5,†], Ning Li[1,2,3,4], Xinyu Shu[1,2,3,4], Lüwen Zhou[1,2,3,4], Shouqin Lü[1,2,3,4], Shenbao Chen[1,2,3,4], Debin Mao[1,2,3,4] and Mian Long[1,2,3,4]

1 Center of Biomechanics and Bioengineering, Institute of Mechanics, Chinese Academy of Sciences, Beijing, China
2 Key Laboratory of Microgravity (National Microgravity Laboratory), Institute of Mechanics, Chinese Academy of Sciences, Beijing, China
3 Beijing Key Laboratory of Engineered Construction and Mechanobiology, Institute of Mechanics, Chinese Academy of Sciences, Beijing, China
4 School of Engineering Science, University of Chinese Academy of Sciences, Beijing, China
5 College of Bioengineering, Chongqing University, China

Keywords
β_2 integrin; allostery; conformational stability; force; salt bridge interaction

Correspondence
S. Lü and M. Long, Institute of Mechanics, Chinese Academy of Sciences, Beijing 100190, China
Fax: +86 10 82543795 (SL); +86 10 82544131 (ML)
Tel: +86 10 82543778 (SL); +86 10 82544131 (ML)
E-mails: lsq@imech.ac.cn (SL); mlong@imech.ac.cn (ML)

[†]These authors contributed equally to this work.

(Received 22 June 2017, revised 23 October 2017, accepted 14 November 2017)

doi:10.1111/febs.14335

The functional performance of the αI domain α_7 helix in β_2 integrin activation depends on the allostery of the α_7 helix, which axially slides down; therefore, it is critical to elucidate what factors regulate the allostery. In this study, we determined that there were two conservative salt bridge interaction pairs that constrain both the upper and bottom ends of the α_7 helix. Molecular dynamics (MD) simulations for three β_2 integrin members, lymphocyte function-associated antigen-1 (LFA-1; $\alpha_L\beta_2$), macrophage-1 antigen (Mac-1; $\alpha_M\beta_2$) and $\alpha_x\beta_2$, indicated that the magnitude of the salt bridge interaction is related to the stability of the αI domain and the strength of the corresponding force-induced allostery. The disruption of the salt bridge interaction, especially with double mutations in both salt bridges, significantly reduced the force-induced allostery time for all three members. The effects of salt bridge interactions of the αI domain α_7 helix on β_2 integrin conformational stability and allostery were experimentally validated using Mac-1 constructs. The results demonstrated that salt bridge mutations did not alter the conformational state of Mac-1, but they did increase the force-induced ligand binding and shear resistance ability, which was consistent with MD simulations. This study offers new insight into the importance of salt bridge interaction constraints of the αI domain α_7 helix and external force for β_2 integrin function.

Introduction

Integrins, a family of cell adhesion molecules, play crucial roles in many physiological and pathological processes by mediating cell–cell or cell–matrix adhesion [1]. Integrins are composed of heterodimeric α and β subunits connected by noncovalent interactions, and they can be divided into two types based on the presence or absence of the αI domain in the α subunit [2]. The αI domain is folded into a spherical conformation with six β sheets (β_1–β_6) and seven α helixes (α_1–α_7), and it protrudes on the head of the integrin with both the N and C termini inserted into a β propeller domain [3,4]. It serves as the key domain for integrin–ligand interactions by directly binding to external ligands. The β_2 integrin subfamily has four members,

Abbreviations
HA, high affinity; IA, intermediate affinity; LA, low affinity; LFA-1, lymphocyte function-associated antigen-1; Mac-1, macrophage-1 antigen; MD, molecular dynamics; MIDAS, metal ion-dependent adhesion site; PCA, principal component analysis; RAGE, receptor for advanced glycation endproducts; SMD, steered molecular dynamics; WT, wild-type.

and they all contain the αI domain in their respective α_L, α_M, α_X or α_D subunit [5]. They are expressed on leukocytes or cancer cells to mediate leukocyte/cancer cell–endothelial cell adhesion in the inflammation cascade [6], lymphocyte homing [7], or cancer metastasis [8] by binding to the corresponding ligands [9,10].

The ligand binding ability of a β_2 integrin is assumed to be determined by its conformational state, which is activated by inside-out or outside-in bidirectional signals [1,2,11]. Three global conformational states of bent-closed, extended-closed and extended-open have been previously reported for β_1, β_2 and β_3 integrins [11–13], which bind corresponding ligands with low affinity (LA), intermediate affinity (IA) and high affinity (HA), respectively [2]. These distinct conformational states of integrins are accompanied by coordinated arrangements of both α and β subunit domains, as well as conformational adjustments of the domain itself. Typically, the αI domain adopts almost intact conformations in both bent-closed and extended-closed states, but the C terminus of the α_7 helix is pulled down along the helical axis in the extended-open state [14]. This movement of the α_7 helix triggers a series of conformational transfers, including the opening of the epitope interface of the αI domain for external ligand and the accessibility of a conserved glutamic acid (Glu) for binding to the metal ion-dependent adhesion site (MIDAS) of the β subunit I domain (βI domain) as the internal ligand [15]. The internal ligand binding further causes global conformational allostery from the closed state to the open state [2]. In other words, pistoning of the αI domain α_7 helix determines the transition of the αI domain between the closed and open states and further governs integrin–ligand binding kinetics for physiological functions.

Allosteric pathways have been extensively investigated with regard to key amino acids. Several static structures of β_2 integrin αI domains in different states have been crystallized with partial or full extracellular domains [3,4,9,15–19]. The extent that the α_7 helix is pulled down corresponds with changes in metal coordination in the MIDAS of the external ligand binding interface and the lateral tilt of both the α_1 helix and the β_6 sheet neighboring the two sides of the α_7 helix. Several key amino acids located on the allosteric regions of the α_1 helix, β_6–α_7 loop and α_7 helix are assumed to be important for regulating the conformation of integrins [14,15,17,20–25]. Alternatively, external force is a physiologically significant mediator for integrin allostery because blood flow or tissue stiffness influences the integrin–ligand complex via cell–cell or cell–matrix adhesion. The catch bond phenomenon of $\alpha_5\beta_1$ [26] and the direct observation of force-induced allostery of lymphocyte function-associated antigen-1 (LFA-1; $\alpha_L\beta_2$) [27] illustrate the importance of external force on integrin conformational dynamics. The mutation of a key residue (R77H) located on the α subunit β propeller of macrophage-1 antigen (Mac-1; $\alpha_M\beta_2$) has no effect on the activation of Mac-1, but it exhibits a significant decrease in ligand binding under shear stress [28]. As the trigger point, it is still far from clear what the regulation factors are and how they affect the pulling down of the αI domain α_7 helix.

Here, we performed equilibration and steered molecular dynamics (SMD) simulations for the αI domains of α_L, α_M and α_X subunits. Two conserved salt bridge interaction pairs, which constrained both the upper part and bottom of the α_7 helix, were validated among the three members. Their corresponding contributions to the α_7 helix being pulled down and further integrin allostery were predicted with simulations of site mutations and then verified using flow cytometry and flow chamber assays with typical Mac-1 constructs. This work extended our understanding of the αI domain α_7 helix flexibility and the structure–function relationships of β_2 integrins under external force.

Results

Conserved salt bridge interactions constrained α_7 helix of β_2 integrin αI domain

The allostery of β_2 integrins mediates the cellular adhesion function by changing the ability to bind to ligands. Pulling down the α_7 helix along the axial vector is pivotal in triggering the conformational regulation of the αI domain and the allosteric transfer from the α subunit to the β subunit. Thus, the freedom of the αI domain α_7 helix is a key factor in regulating the allosteric dynamics of β_2 integrins. We first performed a sequence alignment for all β_2 integrins to evaluate the interaction network of the α_7 helix. The results demonstrated that, except for $\alpha_D\beta_2$, there is a conserved basic residue, Lys/Arg, in the α_1 helix, a conserved acidic residue, Glu/Asp, in the β_6 sheet, and two basic and acidic conserved sites of Lys/Arg and Glu/Asp in the α_7 helix for both humans (Fig. 1A) and mouse (Fig. 1B). Crystallized αI domain structures of $\alpha_L\beta_2$ (Fig. 1C), $\alpha_M\beta_2$ (Fig. 1D) and $\alpha_X\beta_2$ (Fig. 1E) indicated that the β_6 sheet and α_1 helix were located on the left and right sides of the α_7 helix, respectively, and the four conserved residues formed two pairs of salt bridge interactions. One salt bridge interaction between the conserved sites of the α_1 and α_7 helixes was located near the N terminus of the α_7 helix, and the other between the β_6 sheet and the α_7 helix was

located near the C terminus of the α_7 helix (Fig. 1C–E). The constraint of the αI domain α_7 helix by the two conserved salt bridge interaction pairs suggested that these sites may affect the allosteric dynamics and further the ligand-binding ability of β_2 integrins.

Salt bridge interaction strength dominated static stability and force-induced allostery of α_7 helix

To further confirm the existence of the conserved salt bridge interactions and test their effects on α_7 helix stability, we conducted equilibration molecular dynamics (MD) simulations of wild-type (WT) LA αI domains for $\alpha_L\beta_2$, $\alpha_M\beta_2$ and $\alpha_X\beta_2$. The distribution of RMSDs showed that α_7 helix stability was different for the three members. Even based on similar starting crystallized structures, the α_7 helix of α_L was the most flexible and exhibited spontaneous allostery with clearly right-shifted RMSD relative to the LA template (Fig. 2A, black) and left-shifted RMSD relative to the HA template (Fig. 2B, black). α_M (red) and α_X (blue) were comparatively more stable with the lower RMSDs to the LA template (Fig. 2A) and the higher one to the HA template (Fig. 2B). Distance distribution of upper and bottom salt bridge residue pairs showed a similar trend to those of the RMSD distribution (Fig. 2C,D). The most flexible α_L subunit αI domain presented the larger distances for both upper (Fig. 2C, black) and bottom (Fig. 2D, black) salt bridges, while those of comparatively stable α_M and α_X αI domains demonstrated the smaller values (Fig. 2C,D, red and blue). The stability difference among these three systems was also illustrated by principal component analysis (PCA). Both intuitionistic 'porcupine' plots (Fig. 2E) and quantitative eigenvector overlay (Fig. 2F) of the first eigenvector for β_6 sheet and α_7 helix indicated the differences of their intrinsic motion. Corresponding nonbonded interaction energy analyses indicated that the salt bridge interactions proposed by sequence alignment and crystallized structures stably existed in the equilibration MD simulations, which were the main interactions between the α_7 helix and other parts of the αI domain (data not shown). The upper salt bridge interaction energy (black) became stronger from α_L to α_M and to α_X. The bottom salt bridge interaction energy (red) distribution was centralized around -90 kcal·mol^{-1} for all three members, even with different distribution

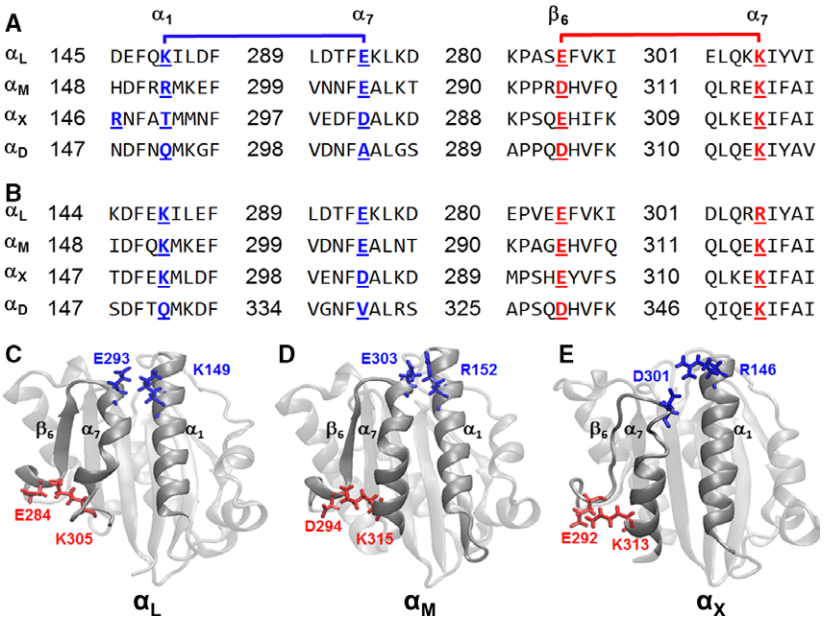

Fig. 1. Sequence alignment of β_2 integrin fragments and the locations of salt bridge interactions between α_7 helix and other parts of αI domain. (A, B) Sequence alignment of α_1 and α_7 helixes and β_6 sheet fragments of αI domain for both human (A) and mouse (B) β_2 integrins. The conserved basic residues of α_1 helix (blue in the left column) and α_7 helix (red in the right column) and the conserved acidic residues of α_7 helix (blue in the second column on the left) and β_6 sheet (red in the third column on the left) are highlighted. (C–E) The locations of two salt bridge interaction pairs in the αI domain of α_L (C) (PDB code 3F74), α_M (D) (PDB code 1JLM) and α_x (E) (PDB code 3K6S) subunits, which are formed by the conserved basic and acidic residues between α_7 helix and α_1 helix (upper salt bridge) or β_6 sheet (bottom salt bridge), respectively. The αI domain and conserved amino acids are presented in silver newcartoon and blue or red licorice, respectively.

frequency and width (Fig. 3A,D,G, red). Pairwise free energy analyses between the α_7 and α_1 helixes and between the α_7 helix and β_6 sheet showed a similar trend to that of nonbonded interaction energy with obvious higher free energy of the two conservative salt bridge residue pairs than other pairwise residues (Fig. 3B,C,E,F,H,I), which further implied that the strong interactions of the two conservative salt bridges are the key factor for inhibiting the allostery of the α_7 helix. It can be noted that the inconsistency between nonbonded energy and pairwise free energy for K287–E301 of the α_L αI domain needs to be further investigated (Fig. 3C). The combination of energy analyses with conformational features indicated that salt bridge interactions dominate the freedom of the α_7 helix and allosteric dynamics.

Steered molecular dynamics simulations were further conducted to verify the contribution of salt bridge interactions to structural stability and allosteric dynamics of the α_7 helix. External forces of 100, 150 and 200 pN were exerted along the α_7 helix axial direction as a driving force to pull it from LA to HA. A typical RMSD evolution of the α_M subunit αI domain α_7 helix relative to LA and HA suggested that the α_7 helix underwent allostery from LA to HA (Fig. 4A). Corresponding evolution of the salt bridge nonbonded interaction energy indicated synchronous disruption at the allosteric moment (Fig. 4B), which demonstrated the importance of salt bridge interactions for maintaining the stability of the α_7 helix. Allosteric time demonstrated a monotonic increase from α_L to α_M to α_X (Fig. 4C). Noting that this difference of allosteric time among three β_2 integrins was similar to that of upper salt bridge interaction energy distribution in equilibration simulations (Fig. 3A,D,G, black), both the equilibrated and steered simulations further supported the dominant role of those salt bridge interactions between the α_7 helix and other parts of the αI domain of β_2 integrins on the stability and allosteric dynamics of the α_7 helix.

Disruption of salt bridge interactions sped up force-induced, but not spontaneous allostery of α_7 helix

Upon correlation of the differences of salt bridge interactions involved in the α_7 helix with the equilibrated

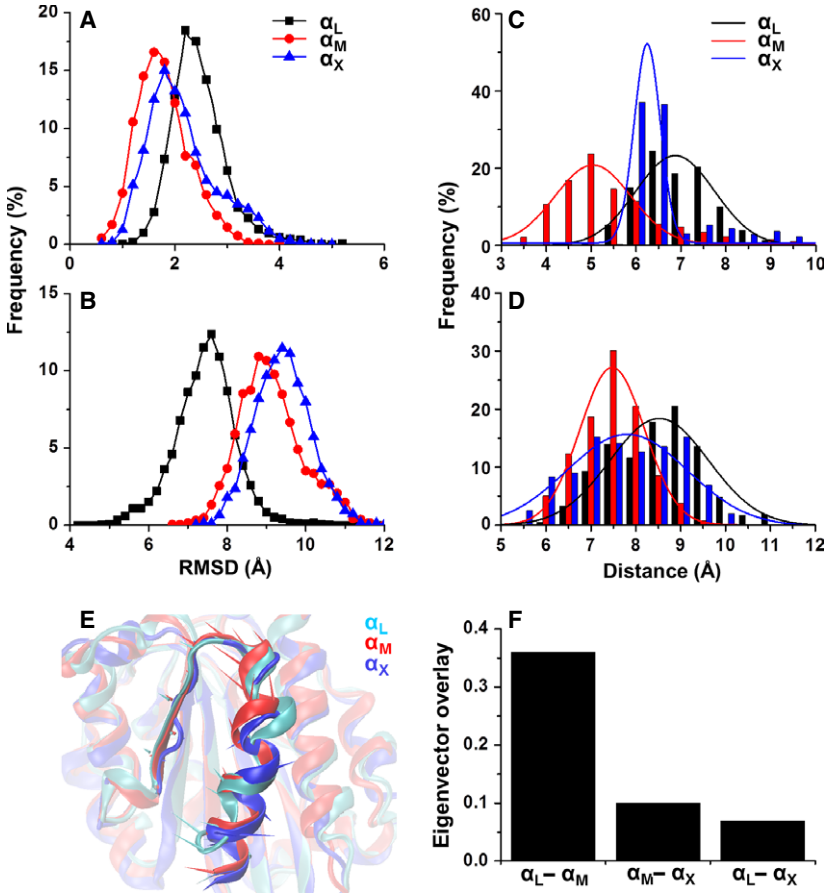

Fig. 2. Stability difference among WT β_2 integrin αI domains in equilibrium simulations. (A, B) α_7 helix RMSD distribution of α_L (black), α_M (red) and α_x (blue) subunit αI domain relative to the template structures of LA 1JLM (A) and HA 1IDO (B), respectively. The backbone RMSD of the α_7 helix was calculated based on the backbone alignment of the core regions of β_1, β_2 and β_4 sheets. (C, D) Distance distribution of upper (C) and bottom (D) salt bridge residue pairs for α_L (black), α_M (red) and α_x (blue) subunit αI domain. The distance was defined as the sidechain geometry center distance of each residue pair. (E, F) Motion difference upon PCA is shown by 'porcupine' plots (E) and pairwise overlap (F) of the first eigenvectors. Only one of three equilibration processes for each system is shown for clarity. The starting points of the 'porcupine' arrows are attached to each C_α atoms of the α_7 helix, and their directions indicate the eigenvector and the magnitude of the corresponding eigenvalue.

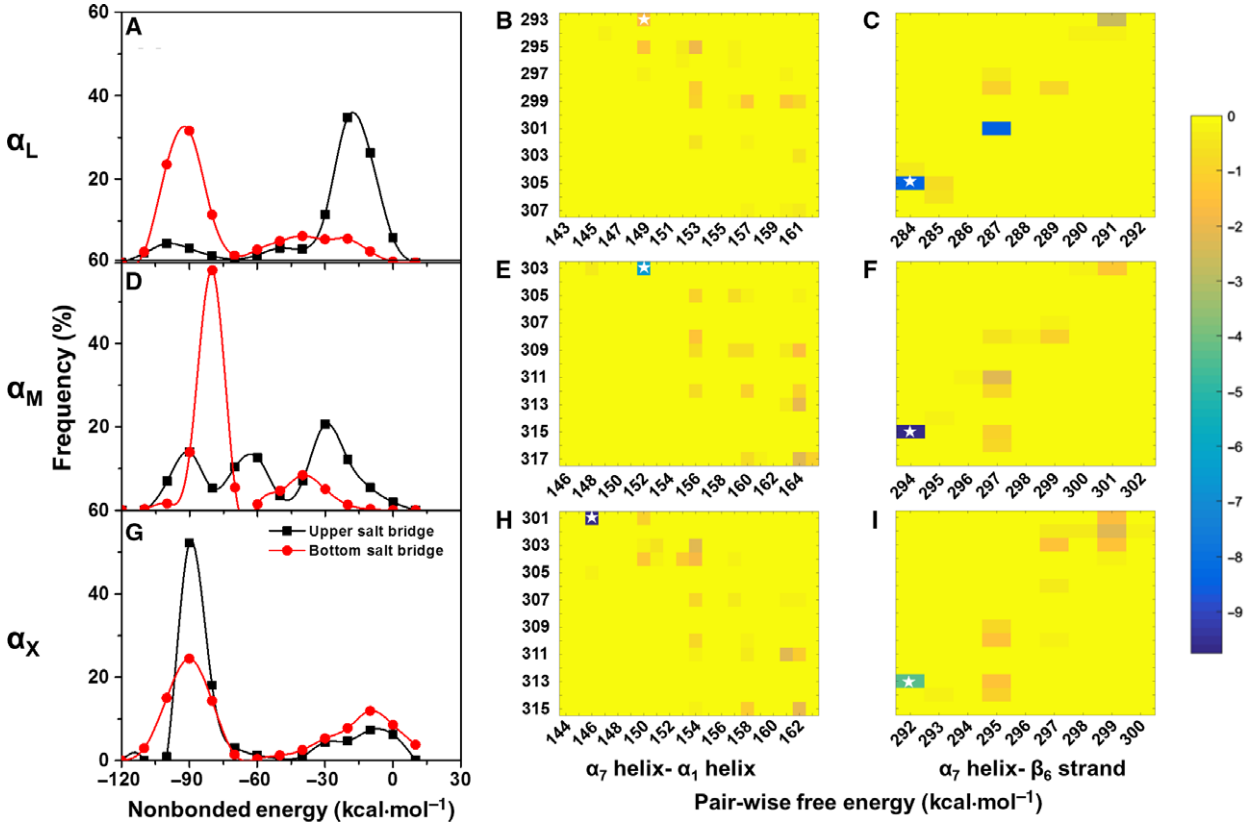

Fig. 3. Distributions of salt bridge interaction energy in equilibrium simulations of WT β_2 integrin αI domains. Nonbond energy (A, D, G) and pairwise free energy (B, C, E, F, H, I) are both presented for α_L (A–C), α_M (D–F) and α_x (G–I) subunit αI domains. Nonbond energy of only upper (black) and bottom (red) salt bridge pairs are presented for clarity. Pairwise free energy between α_7 and α_1 helixes (B, E, H) and between α_7 helix and β_6 sheet (C, F, I) are presented as the mean of three independent simulation runs, and the free energy was calculated for the 100 ns conformational state of each simulation based on the generalized Born solvent model. The corresponding locations of upper and bottom salt bridges for each system are highlighted with a white star in pairwise free energy panels.

stability and force-induced allosteric time among WT β_2 integrins, the above simulations suggested that the existence of stronger salt bridge interactions constrains the flexibility and slows the allostery of the α_7 helix. To confirm this, the influence of salt bridge disruption on the conformational dynamics of mutated α_7 helix was investigated. Three mutation systems were adopted for each β_2 integrin member, which included two independent mutations of either the upper or the bottom salt bridge and mutation of both of them (Table 1). Only the acidic or basic residues of the α_7 helix side involved in salt bridge interactions were mutated to Gly for all mutation systems. The RMSD distribution of equilibration simulations demonstrated that the disruption of salt bridge interactions generally increased the flexibility of the α_7 helix with a broader range than those of WT (black), especially for the bottom salt bridge mutation (blue) and double mutation (green) of both salt bridge interaction pairs (Fig. 5A–F). Although RMSD relative to the HA reference value clearly shifted left for the upper salt bridge mutation (red) of α_M (Fig. 5E) and α_X (Fig. 5F), those relative to the LA reference (Figs. 5B,C) were not significantly different from WT (black). The corresponding superposition of 100 ns snapshots (blue) of double mutation systems with both LA (gray) and HA (red) templates (Fig. 5G–I) illustrates similar structural features to the LA template, except for the deviation of helix orientation and the disruption of helix structure for α_L (Fig. 5G). These equilibration simulations implied that the disruption of salt bridge interactions increases the flexibility but not the spontaneous allostery ability.

Steered molecular dynamics simulations were also conducted to test the effect of salt bridge interaction disruption on force-induced allostery. They indicated that single site mutation of upper or bottom salt bridge interaction pairs did not remarkably change the

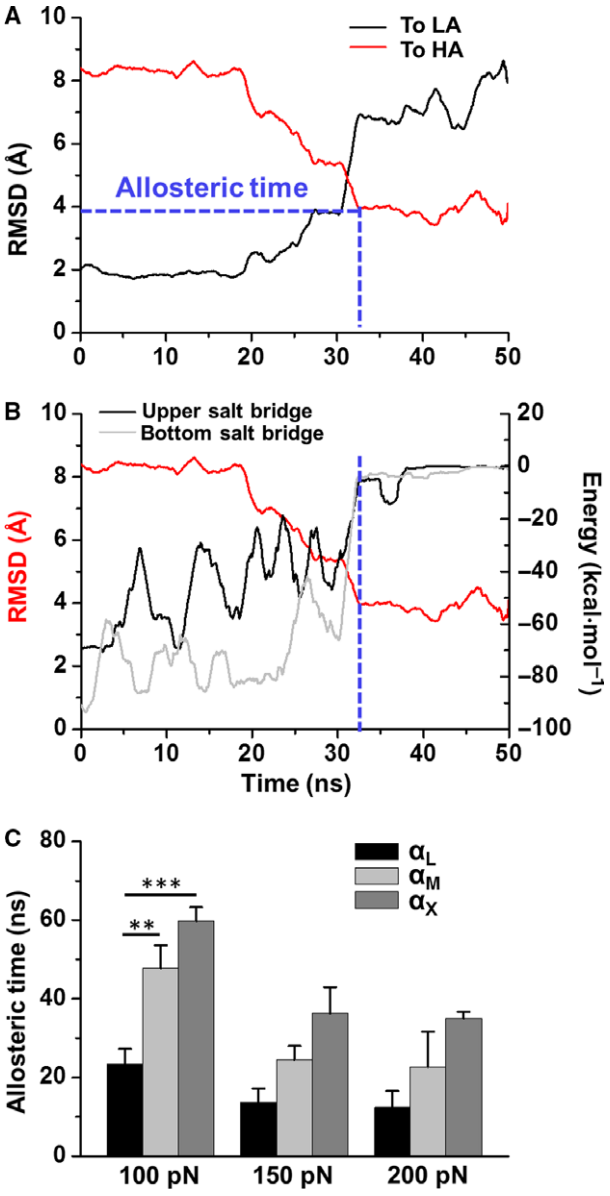

Fig. 4. Conformational evolution and allosteric time comparison of α_7 helix in SMD simulations of WT β_2 integrin αI domains. Evolutions of α_7 helix RMSDs to LA (black) and HA (red) templates and the corresponding upper (black) and bottom (gray) salt bridge nonbonded interactions are shown in (A) and (B), respectively, for one typical steered simulation run of the α_M subunit αI domain. The calculated α_7 helix RMSD and salt bridge nonbonded interaction energy were similar to those in Figs 2 and 3. The allosteric time (dashed blue line in A and B) was defined as the duration between starting time and the moment that the RMSD relative to HA template decreased to less than 4 Å. The RMSD relative to the HA template is also presented in (B) (red) to exhibit a synchronous transition with the salt bridge interactions. Allosteric time comparisons among α_L, α_M and α_X subunit αI domains under different forces of 100, 150 and 200 pN are shown in (C). Each bar represents the mean ± SE of nine independent runs for 100 pN and two runs for 150 and 200 pN; $^{**}P < 0.01$, $^{***}P < 0.001$: paired two-tailed Student's *t* test.

force-induced allosteric time, whereas entire disruption of both salt bridge interaction pairs significantly decreased allosteric time for all three systems. The difference in allosteric time displayed for the three WT systems disappeared (Fig. 6A). RMSD evolution presented visible difference in allosteric time between WT and double mutation systems for α_L (Fig. 6B), α_M (Fig. 6C) and α_X (Fig. 6D) subunit αI domains. Thus, SMD simulation analyses indicated that the disruption of salt bridge interactions speeds up force-induced allostery.

Disruption of salt bridge interactions did not spontaneously activate Mac-1

To further confirm the above predictions that salt bridge interactions locking α_7 helix of β_2 integrin αI domain served as a key factor in regulating structural flexibility and force-induced allostery, human Mac-1–IgG Fc chimera and corresponding mutants were constructed for functional tests. Transfection efficiency and surface presentation on microbeads were confirmed by mean fluorescence intensity) using the fluorescence-activated cell sorting assay (Fig. 7A). The resting conformational states were identified by the reporter of CBRM1/5 mAbs, which distinguishes the HA state of Mac-1 by binding to the activation-specific epitope of the αI domain. The results indicated that the disruption of single or double salt bridge interactions did not activate Mac-1, which yielded a lower binding fraction. By contrast, those positive controls with a HA conformation by disulfide bond locking (Q163C/Q309C) [23] or I316 mutation (K315G/I316G) [14,20,24] presented significantly higher values (Fig. 7B, black bars). Furthermore, additional activation by MEM48 mAbs induced the allostery of WT Mac–Fc from LA conformation to HA conformation (Fig. 7B, gray bar), indicating the reliability of Mac-1–Fc construction without affecting the global and αI domain conformational changes. These results were consistent with the equilibrium MD simulations, in that disruption of salt bridge interactions did not trigger spontaneous allostery.

Disruption of Mac-1 salt bridge interactions favored force-induced ligand binding

To further understand whether the salt bridge interactions of Mac-1 played a role in adhesion between leukocytes and endothelial cells under blood flow, an *in vitro* flow chamber assay was used to test the adhesion dynamics of Mac-1–Fc-coated microbeads to ligand-immobilized substrate under either a constant

Table 1. Summary of the simulation set-up. Eq, equilibration.

		Simulations (duration (ns) × runs)											
		Free MD				Steered MD							
						WT					Mutant		
			Mutant			Eq-1			Eq-2	Eq-3	Upper	Bottom	Double
System	PDB code	WT	Upper	Bottom	Double	100 pN	150 pN	200 pN	100 pN	100 pN	100 pN	100 pN	100 pN
LFA-1	3F74	100 × 3	100 × 3	100 × 3	100 × 3	40 × 1	20 × 1	20 × 1	60 × 1	50 × 1	40 × 1	30 × 1	30 × 1
						50 × 1	15 × 1	15 × 1	50 × 1	60 × 1	50 × 1	40 × 1	30 × 1
						70 × 1			70 × 1	60 × 1	30 × 1	30 × 1	30 × 1
Mac-1	1JLM	100 × 3	100 × 3	100 × 3	100 × 3	90 × 1	30 × 1	20 × 1	60 × 1	70 × 1	60 × 1	60 × 1	50 × 1
						50 × 1	30 × 1	35 × 1	50 × 1	70 × 1	90 × 1	50 × 1	50 × 1
						70 × 1			50 × 1	70 × 1	50 × 1	40 × 1	50 × 1
$\alpha_x\beta_2$	3K6S	100 × 3	100 × 3	100 × 3	100 × 3	60 × 1	45 × 1	40 × 1	70 × 1	80 × 1	50 × 1	60 × 1	40 × 1
						60 × 1	35 × 1	40 × 1	70 × 1	80 × 1	40 × 1	60 × 1	40 × 1
						60 × 1			70 × 1	70 × 1	60 × 1	60 × 1	40 × 1

shear stress of 0.5 dyn·cm^{-2} or under a stepwise increased shear stresses of 1–48 dyn·cm^{-2} (Fig. 7C). At similar site densities of Mac-1–Fc constructs on microbeads (Fig. 7A) and comparable coating densities of the ligand receptor for advanced glycation endproducts (RAGE) on substrate, the reliability and sensitivity of the flow assay was verified. Here, higher adhesion efficiency and resistance strength were observed for binding of those microbeads coated with HA mutants (Q163C/Q309C and K315G/I316G) to RAGE ligands (Fig. 7D,E) than those for WT constructs and negative control coated with plain transfection supernatant of p3.1. WT constructs also demonstrated significant higher values than those from the control. We further compared the adhesion dynamics mediated by salt bridge interaction mutants with those mediated by the Q163C/Q309C mutant. The results showed that the double mutant for salt bridge interactions (E303G/K315G) (blue) mediated more preferable adhesion, with a quicker increase of bound microbeads in time-lapsed adhesion and a slower reduction of bound microbeads in stress-dependent resistance than those for the Q163C/Q309C mutant (black) when binding to RAGE ligands (Fig. 7F,G). Although the single site mutation of E303G (red) involved in upper salt bridge interactions mediated lower time-lapsed adhesion than that of Q163C/Q309C (Fig. 7F), the increase of bound microbeads was still quicker than WT with more adhesion at the last three time points (Fig. 7D,F, red). Furthermore, E303G exhibited comparable stress-dependent resistance ability to that of Q163C/Q309C (Fig. 7G). These results indicated that the disruption of salt bridge interactions favored force-induced allostery, which was consistent with the prediction from the SMD simulations.

Discussion

The αI domain protrudes from the top of the α subunit with the N and C termini inserted into the β propeller domain. The function of the αI domain as an internal ligand is determined by the sliding down of the α_7 helix along the helix axis, which also closely correlates with conformational rearrangement of the binding interface for external ligands. Thus, the ability and difficulty of pulling the α_7 helix down dominates the allosteric effect and dynamics. In this study, we unraveled two pairs of conservative salt bridge interactions for all four β_2 integrin members, which are located on the upper and bottom α_7 helix of the αI domain (Fig. 1). Free and steered MD simulations of α_L, α_M and α_X αI domains indicated that differences in salt bridge interaction strength among the three systems was directly proportional to differences in α_7 helix stability and force-induced allosteric dynamics (Figs 2–4). The complete disruption of these salt bridge interactions significantly decreased force-induced allosteric times and erased the initial differences, but it had no effect on spontaneous allostery, except increased flexibility (Figs 5 and 6). Conformational tests and the flow-induced binding ability of Mac-1–Fc constructs evaluated by combining flow cytometry with a flow chamber assay provided results consistent with those of the simulations (Fig. 7).

Allosteric ability and dynamics of integrins are two important factors related to the biological functions of integrins. The former is embodied in disruption of the

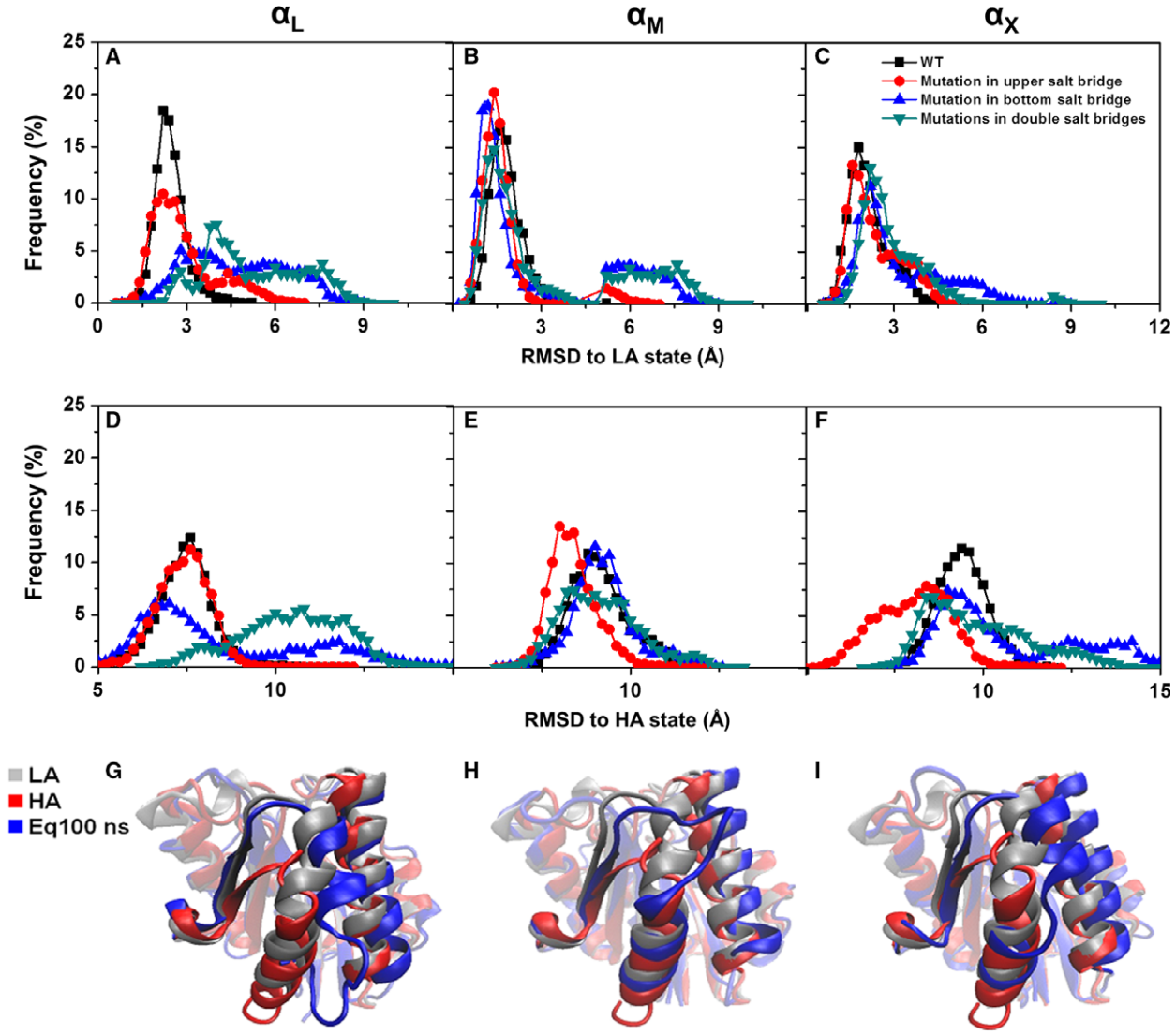

Fig. 5. α_7 helix RMSD distribution in equilibrium simulations for salt bridge mutants of β_2 integrin αI domains. (A–F) α_7 helix RMSD distribution of WT and mutants relative to LA (A–C) and HA (D–F) templates for α_L (A, D), α_M (B, E) and α_X subunit (C, F) αI domains. The corresponding residue sites of the α_7 helix involved in salt bridge interactions were mutated to Gly, and the mutants included two single mutations in the upper (blue) or bottom (red) salt bridge and one double mutation in both the upper and the bottom (green) salt bridge. The α_7 helix RMSD of WT (black) is presented for comparison. The calculation of α_7 helix RMSD was similar to those in Fig. 2, and the data were collected from three independent simulation runs for each system. (G–I) Intuitive conformation comparisons are shown among LA (silver) and HA (red) templates and one typical 100 ns snapshot of the double mutation (blue) for α_L (G), α_M (H) and α_X (I) subunit αI domain.

hydrophobic interaction through which a conserved Ile site is mutated and the disulfide bond locks the α_7 helix; both of these change the closed conformation state to an open one and consequentially increase integrin–ligand binding affinity [14,20,21,23,24]. Data with the Mac-1–Fc Q163C/Q309C and K315G/I316G mutants were consistent with previous observations that showed significantly increased binding to CRBM1/5 (Fig. 7B) and quicker ligand binding and stronger shear resistance (Figs. 7D,E). It is also interesting that all mutations involved in salt bridge interactions did not alter the conformational state of Mac-1, which had a comparable CRBM1/5 binding fraction to that of WT (Fig. 7B). By contrast, force-induced ligand binding and shear resistance were significantly enhanced, compared with WT, when binding to RAGE ligands. Specifically, the double mutation E303G/K315G, which was involved in two pairs of salt bridge interactions, even provided greater affinity for ligands in comparison with the Q163C/Q309C

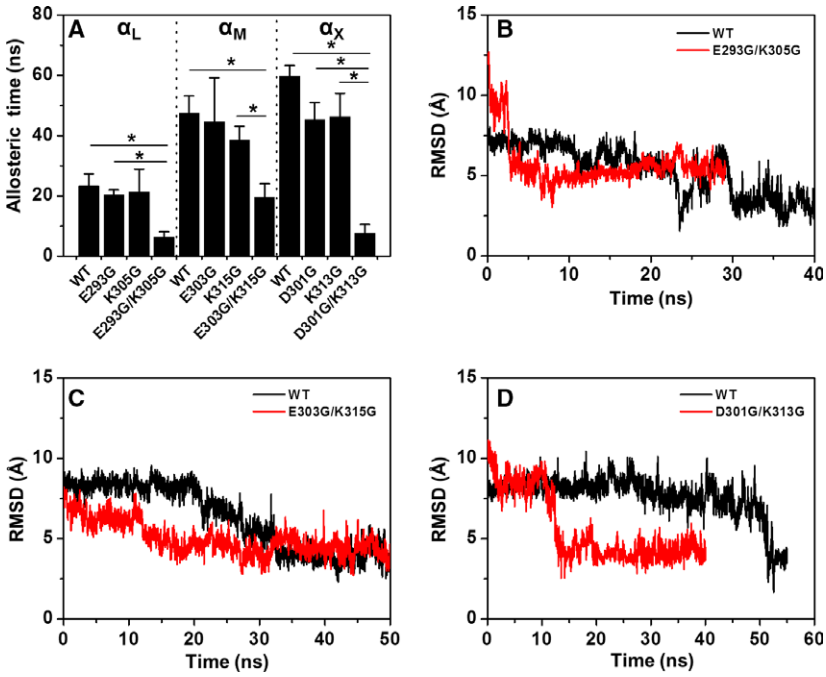

Fig. 6. Allosteric dynamics comparisons between WT and salt bridge mutants for β_2 integrin αI domains. (A) Quantitative comparison of allosteric time between WT and upper, bottom or double salt bridge mutants for α_L (left bars), α_M (middle bars) and α_X (right bars) subunit αI domains. Each bar represents the mean ± SE of nine runs for WTs and three runs for mutants; $^*P < 0.05$. (B–D) α_7 helix RMSD evolution comparison of typical SMD simulations between WT and double mutant for α_L (B), α_M (C) and α_X (D) subunit αI domains, respectively. Only RMSDs relative to HA templates are shown for clarity.

construct (Fig. 7F,G). These results indicated that external forces induce easily accessible allostery for mutants disrupting the salt bridge, since these disruptions enhance the freedom of the α_7 helix and speed up the allostery, as observed with the forced allostery of the Mac-1 R77H mutant [28]. β_2 integrin–ligand binding kinetics and the corresponding conformational features have been employed to clarify the differences of activation dynamics and biological function between LFA-1 and Mac-1. LFA-1 has a higher binding affinity to intercellular adhesion molecule-1 than Mac-1, which has an on-rate dominated by a slightly or moderately varied off-rate [29]. Related structural analyses using MD simulations show that LFA-1 has a less stable αI domain α_7 helix and then presents spontaneous allostery from the LA to IA affinity states compared with Mac-1 [30]. Thus, distinct features are consistent with their distinct biological functions in LFA-1 initiating polymorphonuclear leukocyte slow rolling and firm adhesion and in Mac-1-mediating cell crawling. The difference in conserved salt bridge interactions involved in the α_7 helix and their effect on αI domain stability and force-induced allostery observed in this study offered an intrinsic structural mechanism to explain the difference between LFA-1 and Mac-1.

Salt bridge interactions in the αI domain α_7 helix of the β_2 integrin are further confirmed by X-ray crystals of LFA-1 head domains [4] and closed $\alpha_x\beta_2$ [3], and the disappearance of salt bridge interactions in the HA Mac-1 I domain [18] and internal ligand bound $\alpha_x\beta_2$ [15] structures indicate that the allostery of the αI domain disrupts the salt bridge interactions. This study demonstrated the importance of external forces on the disruption of the salt bridge interaction and β_2 integrin allostery. Intriguingly, the salt bridge interactions of the αI domain α_7 helix of β_2 integrins are not conserved in other αI domain-containing integrins, as well as the βI-like domains, even though the βI-like domains have similar conformations to those of αI domains. These differences suggest various allosteric dynamics among integrin members.

The effect of the key residues involved in conserved salt bridge interactions was evaluated with corresponding mutations to Gly in both simulations and experiments to maintain similar polarity but decrease the charge. Gly can also disrupt the secondary structure of helixes, and the mutations of charged basic or acidic residues to Gly would possibly destroy the salt bridge interactions by perturbing the structure of the α_7 helix. Our simulations demonstrated that mutation to Gly did not clearly disrupt the α_7 helix structure (Fig. 5), so the increased force-induced allostery for mutations of double salt bridge interactions mainly resulted from salt bridge interactions. In fact, the importance of the residues involved in conserved salt bridge interactions have been reported previously. In the absence of external force, the mutation of LFA-1 K305 to Ala decreases ligand-binding affinity [20], and the mutation $\alpha_X\beta_2$ K313I destabilizes internal ligand binding and, hence, allostery relay [15]. The inconsistency between

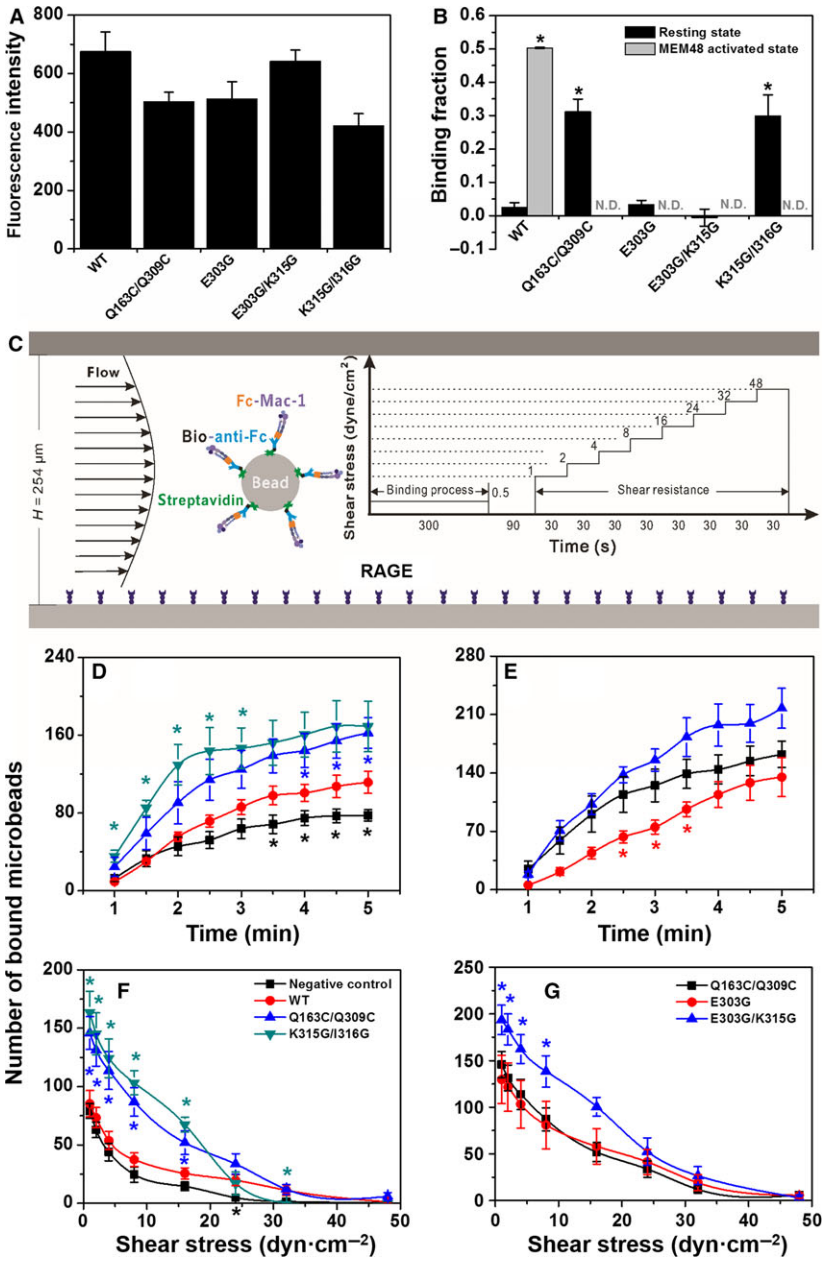

Fig. 7. Protein reconstruction and functional tests of Mac-1–Fc WT and mutants. (A) Quantification of surface presentation of distinct Mac-1–Fc constructs by fluorescence intensity. (B) Conformational comparison between WT and mutants was determined using CBRM1/5 binding fraction. (C) Schematic depiction of functionalized microbeads and substrate with time course of shear flow specified as inset. The number of bound microbeads in a time-lapse course at 0.5 dyn·cm^{-2} shear stress (D, F) or in a stress-dependent course at 30 s shear duration (E, G) are plotted for the binding specificity validation (D, E) and evaluation of salt bridge mutation (F, G). Data are shown as the mean ± SE of at least three runs. Paired two-tailed Student's *t* tests were performed for the data for WT in (D, E) and for Q163C/Q309C in (F, G); $*P < 0.05$.

those two cases and this study indicates the importance of external force in the function of β_2 integrins.

Schematically, bound microbeads mediated by the β_2 integrin–ligand interaction complex under shear flow are able to transfer external forces to the complex. The same external force induces greater pulling down of the αI domain α_7 helix for those constructs with disrupted salt bridge constraints than for the WT construct with the intact salt bridge constraint. Disrupting salt bridge interactions increases the freedom and flexibility of the α_7 helix, which accelerates allostery of the α_7 helix and the conformational regulation of the αI domain with greater affinity for external ligand binding (Fig. 8). Taken together, our data suggest that different salt bridge interactions that lock the αI domain α_7 helix might suggest intrinsic mechanisms to explain structural and functional differences among β_2 integrins, although the corresponding strengths of salt bridge interactions among β_2 integrins require further investigation. Considering the effects of salt bridge disruption on spontaneous and force-induced allostery of Mac-1 constructs, this work also promotes our understanding of allosteric dynamics in αI domain-containing integrins.

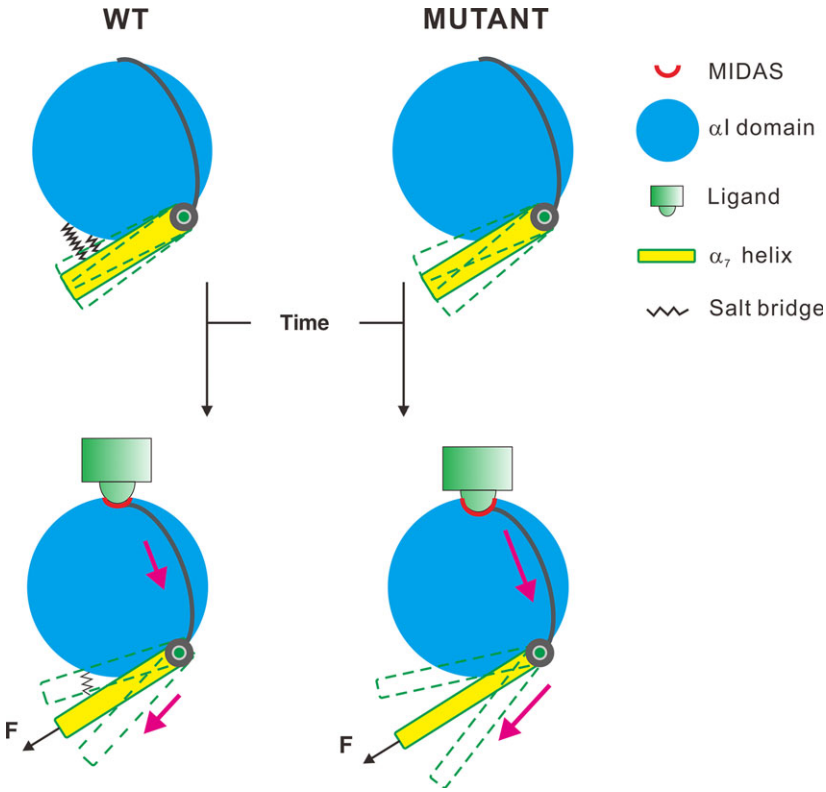

Fig. 8. Working model for the effect of salt bridge interactions on force-induced αI domain allostery and ligand binding. Release of salt bridge interaction constraints of the α_7 helix resulted in higher freedom and greater allosteric movement of β_2 integrin αI domain α_7 helix under the same external force and time, which led to stronger ligand binding and shear resistance.

Materials and methods

Molecular dynamics simulations

System construction

Low affinity αI domains (LFA-1/3F74 [16], Mac-1/1JLM [9], $\alpha_X\beta_2$/3K6S [3]) and respective salt bridge interaction mutants of three β_2 integrin members were employed in the MD simulations. The metal ion in MIDAS was set as Ca^{2+} for all systems by replacing the Mn^{2+} ion of 1JLM. Each simulation system was built up by solvating the target molecule(s) in a rectangular water box and neutralized with ~ 100 mM Na^+ and Cl^- ions. The NAMD program [31] with CHARMM27 all-atom force field [32] was used for the simulations.

Equilibration and steered MD simulations

An integration time step of 1 fs and periodic boundary conditions were applied in the simulations. A smooth (10–12 Å) cutoff and the particle mesh Ewald method were employed to calculate van der Waals forces and full electrostatics, respectively. A 300 K heat bath was manipulated using a Langevin thermostat, and 1 atm pressure was controlled by the Nosé–Hoover Langevin piston method. Prior to the equilibration process, energy minimization with 10 000 steps of fixed backbone atoms was followed by an additional 10 000 steps with all atoms free, and the system was heated from 0 to 300 K by 30 K increments every 5 ps. Three independent equilibration runs of 100 ns were performed for each system. Then, SMD simulations were conducted based on the final state of respective 100 ns equilibration to force the allostery of the αI domain α_7 helix from LA to HA. Here, the backbone atoms of the αI domain stable core of β_1, β_2 and β_4 sheets were fixed and a constant force of 100/150/200 pN was applied on the C-terminal C_α atom of the α_7 helix. The force direction was along the vector from the atomic geometry center of A303-C_α to that of N310-C_α of the reference HA Mac-1 αI domain after aligning the stable core backbone to the target 100 ns equilibration snapshot. The forced amino acids were Y307, A318 and A316 for LFA-1, Mac-1 and $\alpha_X\beta_2$ αI domains, respectively. At least two independent SMD simulation runs were performed for each system. The simulation set-up in this study is summarized in Table 1. All 3600 ns equilibration and 3315 ns SMD simulations were performed in this study.

Structural analyses

The RMSD of the α_7 helix was used to quantify the stability of the αI domain and the allostery by aligning different reference structures of LA (1JLM), IA (1MJN) and HA (1IDO) αI domains. Distance between the salt bridge

residue pair was also calculated for the equilibration simulations of WT systems to quantify the stability of the αI domain. Energy analyses, including nonbonded interaction and pairwise free energy, were carried out for quantifying the interaction strength between the α_7 helix and other parts of the αI domain, especially for the upper and bottom salt bridge interactions between α_7 and α_1 helixes and between the α_7 helix and β_6 sheet. Pairwise free energy decomposition was calculated using the MMPBSA module of AMBERTOOLS15 [33], based on the generalized Born model [34]. Essential motion patterns were quantified by PCA for WT equilibration simulations. All system construction, residue site mutations, structural analyses and visualization were performed using the VMD program [35].

Protein reconstruction

A soluble human Mac-1–IgG Fc chimera (Mac-1–Fc) was constructed as previously described [29]. A series of mutations (Q163C/Q309C, E303G, E303G/K315G, K315G/I316G) were generated by the QuikChange Lightning site-directed mutagenesis kit (Agilent, Santa Clara, CA, USA) and verified by DNA sequencing (data not shown). The plasmids were transfected into 293T cells via a calcium phosphate-mediated transfection procedure (Promega, Madison, WI, USA), and the supernatant was collected by centrifugation at 1000 ***g*** for 20 min after 96 h culture. Soluble Mac-1–Fc chimeras were harvested via biotin-conjugated anti-IgG-Fc secondary antibody (Santa Cruz Biotechnology, Santa Cruz, CA, USA), which was precoated on streptavidin-modified microbeads (Bangs Laboratories, Fishers, IN, USA). A conformational test of Mac-1 WT and mutations was conducted using flow cytometry and activation reporter antibody. Two aliquots of Mac-1–Fc captured microbeads were incubated with fluorescein isothiocyanate-conjugated anti-CD11b (clones of CBRM1/5 and TS1/18) mAbs (Santa Cruz Biotechnology) at a concentration of 10 $\mu g \cdot mL^{-1}$ for 30 min on ice. Washed microbeads were analyzed by flow cytometry (BD Biosciences, San Jose, CA, USA). The fraction of activated Mac-1 (CBRM1/5 binding) was estimated as the fraction of the total Mac-1 (TS1/18 binding) using the equation of $(B_p - B_{ctrl})/(E_p - E_{ctrl})$, where B_p and E_p are the amounts of CBRM1/5 and TS1/18 binding, respectively, and B_{ctrl} and E_{ctrl} denoted the amounts of negative control (mock transfected supernatant) of CBRM1/5 and TS1/18 binding, respectively. The activation effects of MEM48 mAbs (Santa Cruz Biotechnology) were also tested using the same reporter of CBRM1/5 mAbs after the incubation of MEM48.

Flow chamber assay

A parallel-plate flow chamber assay was used to test the ligand-binding difference among Mac-1–Fc constructs with a circular GlycoTech flow cell system (no. 31-001, Gaithersburg, MD, USA) assembled into a flow chamber with length 2 cm × width 0.5 cm × height 0.01 inch. RAGE (10 $\mu g \cdot \mu L^{-1}$) ligands were coated on a sterile 35-mm tissue culture dish by physical absorption. Briefly, 15 μL RAGE was incubated on an area of 0.5 × 0.5 cm for 2 h at 37°C. The coating area was then washed with PBS three times, followed by blocking incubation with 1% BSA (Beijing SeaskyBiotechnology Co. Ltd, Beijing, China) for 2 h at 37 °C. Flowing microbeads were coated with purified Mac-1–Fc constructs for a final concentration of 1.3–1.7 × $10^6 \cdot mL^{-1}$. Briefly, 100 μL streptavidin-modified 5-μm glass microbeads in 400 μL PBS dilution were incubated with 2 μL (400 $\mu g \cdot mL^{-1}$) biotin-conjugated goat-anti-human IgG-Fc antibody and shaken for 4 h. After three times PBS washing, 400 μL Mac-1–Fc transfection supernatant was added to 100 μL of the prepared solution for 12 h at 4 °C at 180 r.p.m. After three times PBS washing, followed by blocking with 1% BSA for 2 h at 37 °C, the collected microbeads were ready for flow chamber assay. Those microbeads coated by blank transfection supernatant were used as a control.

The flow chamber test included two sequential phases (Fig. 7C). The first focused on the investigation of Mac-1–ligand-binding ability by refilling the microbead solution and counting the number of adhered microbeads under a constant shear stress of 0.5 $dyn \cdot cm^{-2}$ for 5 min. The second was performed by following the first phase by switching the refilling microbead solution to blank HBSS solution with a stepwise shear stress from 1 to 48 $dyn \cdot cm^{-2}$ with 30 s for each stress. The number of microbeads remaining adhered 30 s after each stress was counted to quantify the shear resistance of Mac-1–ligand interaction. At least three independent tests with at least two distinct protein transfections were performed for each Mac-1–Fc recombinant.

Acknowledgements

MD simulations were performed at the National Supercomputer Center in Tianjin. This work was supported by National Natural Science Foundation of China (grant numbers 31230027, 91642203, and 11372332); National Key Research and Development Program of China (grant number 2016YFA0501601); and Strategic Priority Research Program of Chinese Academy of Sciences (grant number XDB22040101).

Conflicts of interest

XZ, LL, NL, XS, LZ, SL, SC, DM and ML declare that they have no conflict of interest. All institutional and national guidelines for the care and use of laboratory animals were followed.

Author contributions

XZ performed the MD simulations, analyzed the data, prepared the figures and wrote the article. LL performed the flow chamber experiments and analyzed the data. NL and XS designed and constructed vectors for expression of Mac-1–Fc proteins. LZ analyzed the data of the flow chamber experiments. SL analyzed and interpreted the data, and drafted the article. SC interpreted the MD simulation and flow chamber data, and prepared the figures. DM performed the MD simulations. ML designed the study, revised the paper and approved the final version of the article for publication. All authors reviewed the results and approved the final version of the manuscript.

References

1 Hynes RO (2002) Integrins: bidirectional, allosteric signaling machines. *Cell* **110**, 673–687.

2 Luo BH, Carman CV & Springer TA (2007) Structural basis of integrin regulation and signaling. *Annu Rev Immunol* **25**, 619–647.

3 Xie C, Zhu J, Chen X, Mi L, Nishida N & Springer TA (2010) Structure of an integrin with an alphaI domain, complement receptor type 4. *EMBO J* **29**, 666–679.

4 Sen M & Springer TA (2016) Leukocyte integrin alphaLbeta2 headpiece structures: the alphaI domain, the pocket for the internal ligand, and concerted movements of its loops. *Proc Natl Acad Sci USA* **113**, 2940–2945.

5 Tan SM (2012) The leucocyte beta2 (CD18) integrins: the structure, functional regulation and signalling properties. *Biosci Rep* **32**, 241–269.

6 Ley K, Laudanna C, Cybulsky MI & Nourshargh S (2007) Getting to the site of inflammation: the leukocyte adhesion cascade updated. *Nat Rev Immunol* **7**, 678–689.

7 Robinson MK, Andrew D, Rosen H, Brown D, Ortlepp S, Stephens P & Butcher EC (1992) Antibody against the Leu-Cam beta-chain (Cd18) promotes both LFA-1-dependent and cr3-dependent adhesion events. *J Immunol* **148**, 1080–1085.

8 Slattery MJ & Dong C (2003) Neutrophils influence melanoma adhesion and migration under flow conditions. *Int J Cancer* **106**, 713–722.

9 Lee JO, Bankston LA, Arnaout MA & Liddington RC (1995) Two conformations of the integrin A-domain (I-domain): a pathway for activation? *Structure* **3**, 1333–1340.

10 Mehrbod M, Trisno S & Mofrad MR (2013) On the activation of integrin alphaIIbbeta3: outside-in and inside-out pathways. *Biophys J* **105**, 1304–1315.

11 Takagi J, Petre BM, Walz T & Springer TA (2002) Global conformational rearrangements in integrin extracellular domains in outside-in and inside-out signaling. *Cell* **110**, 599–611.

12 Su Y, Xia W, Li J, Walz T, Humphries MJ, Vestweber D, Cabanas C, Lu C & Springer TA (2016) Relating conformation to function in integrin alpha5beta1. *Proc Natl Acad Sci USA* **113**, E3872–E3881.

13 Chen X, Xie C, Nishida N, Li Z, Walz T & Springer TA (2010) Requirement of open headpiece conformation for activation of leukocyte integrin alphaXbeta2. *Proc Natl Acad Sci USA* **107**, 14727–14732.

14 Xiong JP, Li R, Essafi M, Stehle T & Arnaout MA (2000) An isoleucine-based allosteric switch controls affinity and shape shifting in integrin CD11b A-domain. *J Biol Chem* **275**, 38762–38767.

15 Sen M, Yuki K & Springer TA (2013) An internal ligand-bound, metastable state of a leukocyte integrin, alphaXbeta2. *J Cell Biol* **203**, 629–642.

16 Zhang H, Astrof NS, Liu JH, Wang JH & Shimaoka M (2009) Crystal structure of isoflurane bound to integrin LFA-1 supports a unified mechanism of volatile anesthetic action in the immune and central nervous systems. *FASEB J* **23**, 2735–2740.

17 Shimaoka M, Xiao T, Liu JH, Yang Y, Dong Y, Jun CD, McCormack A, Zhang R, Joachimiak A, Takagi J *et al.* (2003) Structures of the αL I domain and its complex with ICAM-1 reveal a shape-shifting pathway for integrin regulation. *Cell* **112**, 99–111.

18 Lee JO, Rieu P, Arnaout MA & Liddington R (1995) Crystal structure of the A domain from the a subunit of integrin CR3 (CD11 b/CD18). *Cell* **80**, 631–638.

19 Song G, Yang Y, Liu JH, Casasnovas JM, Shimaoka M, Springer TA & Wang JH (2005) An atomic resolution view of ICAM recognition in a complex between the binding domains of ICAM-3 and integrin alphaLbeta2. *Proc Natl Acad Sci USA* **102**, 3366–3371.

20 Huth JR, Olejniczak ET, Mendoza R, Liang H, Harris EAS, Lupher ML, Wilson AE, Fesik SW & Staunton DE (2000) NMR and mutagenesis evidence for an I domain allosteric site that regulates lymphocyte function-associated antigen 1 ligand binding. *Proc Natl Acad Sci USA* **97**, 5231–5236.

21 Shimaoka M, Lu C, Palframan RT, von Andrian UH, McCormack A, Takagi J & Springer TA (2001) Reversibly locking a protein fold in an active conformation with a disulfide bond: integrin alphaL I domains with high affinity and antagonist activity in vivo. *Proc Natl Acad Sci USA* **98**, 6009–6014.

22 Jin M, Song G, Carman CV, Kim YS, Astrof NS, Shimaoka M, Wittrup DK & Springer TA (2006) Directed evolution to probe protein allostery and integrin I domains of 200,000-fold higher affinity. *Proc Natl Acad Sci USA* **103**, 5758–5763.

23 Shimaoka M, Lu C, Salas A, Xiao T, Takagi J & Springer TA (2002) Stabilizing the integrin alpha M

inserted domain in alternative conformations with a range of engineered disulfide bonds. *Proc Natl Acad Sci USA* **99**, 16737–16741.

24 Vorup-Jensen T, Ostermeier C, Shimaoka M, Hommel U & Springer TA (2003) Structure and allosteric regulation of the alpha X beta 2 integrin I domain. *Proc Natl Acad Sci USA* **100**, 1873–1878.

25 Choi J, Choi J & Nham SU (2010) Characterization of the residues of alphaX I-domain and ICAM-1 mediating their interactions. *Mol Cells* **30**, 227–234.

26 Kong F, Garcia AJ, Mould AP, Humphries MJ & Zhu C (2009) Demonstration of catch bonds between an integrin and its ligand. *J Cell Biol* **185**, 1275–1284.

27 Chen W, Lou J, Evans EA & Zhu C (2012) Observing force-regulated conformational changes and ligand dissociation from a single integrin on cells. *J Cell Biol* **199**, 497–512.

28 Rosetti F, Chen Y, Sen M, Thayer E, Azcutia V, Herter JM, Luscinskas FW, Cullere X, Zhu C & Mayadas TN (2015) A lupus-associated Mac-1 variant has defects in integrin allostery and interaction with ligands under force. *Cell Rep* **10**, 1655–1664.

29 Li N, Mao DB, Lü SQ, Tong CF, Zhang Y & Long M (2013) Distinct binding affinities of Mac-1 and LFA-1 in neutrophil activation. *J Immunol* **190**, 4371–4381.

30 Mao DB, Lü SQ, Li N, Zhang Y & Long M (2011) Conformational stability analyses of alpha subunit I domain of LFA-1 and Mac-1. *PLoS One* **6**, e24188.

31 Phillips JC, Braun R, Wang W, Gumbart J, Tajkhorshid E, Villa E, Chipot C, Skeel RD, Kale L & Schulten K (2005) Scalable molecular dynamics with NAMD. *J Comput Chem* **26**, 1781–1802.

32 MacKerell AD, Bashford D, Bellott M, Dunbrack RL, Evanseck JD, Field MJ, Fischer S, Gao J, Guo H, Ha S *et al.* (1998) All-atom empirical potential for molecular modeling and dynamics studies of proteins. *J Phys Chem B* **102**, 3586–3616.

33 Case DA, Berryman JT, Betz RM, Cerutti DS, Cheatham TE III, Darden TA, Duke RE, Giese TJ, Gohlke H, Goetz AW *et al.* (2015) AMBER 2015. University of California, San Francisco, San Francisco, CA.

34 Matthew CL, Rong Y & Yong D (2005) Comparison between Generalized-Born and Poisson–Boltzmann methods in physics-based scoring functions for protein structure prediction. *J Mol Model* **12**, 101–110.

35 Humphrey W, Dalke A & Schulten K (1996) VMD: visual molecular dynamics. *J Mol Graph* **14**, 27–38.